Mechanisms in ^{3}H + ^{3}He and ^{3}H + ^{2}H Reactions

Ivo Slaus

Institute R. Bošković, Zagreb, Yugoslavia and Naval Research Laboratory, Washington, D. C. 20375

and

R. G. Allas, L. A. Beach, R. O. Bondelid, and E. L. Petersen

Naval Research Laboratory, Washington, D. C. 20375

and

J. M. Lambert

Georgetown University, Washington, D. C. 20007, and Naval Research Laboratory, Washington, D. C. 20375

and

D. L. Shannon

University of California, Los Angeles, California 90024

The study of ^{3}H + ^{3}He reactions at $E_{^3\text{He}} = 50$ MeV, ^{3}H + ^{2}H reactions at $E_d = 35$ MeV, as well as the reanalysis of ^{2}H(^{3}He, pt)p reaction demonstrates that the quasifree reaction mechanism plays an important role. Evidence for the quasifree reaction mechanism is found in the processes ^{3}H(^{3}He, dd)d, ^{3}H(^{3}He, pt)d, ^{3}H(^{3}He, dt)p, ^{3}H(^{3}He, $p\alpha$)n, ^{2}H(^{3}He, pt)p, and ^{3}H(^{2}H, pt)n. Evidence for d-d, p-^{3}He, d-^{3}He, and p-t quasifree scattering is found in the processes ^{3}H(^{2}H, dd)n, ^{3}H(^{3}He, p^3He)$2n$, ^{3}H(^{3}He, d^3He)n, and ^{3}H(^{2}H, pt)n, respectively. Comparing the absolute cross sections of these reactions, one concludes that though the shapes of the correlation spectra indicate the significance of quasifree reaction mechanisms, the pole diagram is not dominant.

I. INTRODUCTION

Multiparticle reactions have provided important information on nuclear structure and nuclear reaction mechanisms. One of the simplest of these reactions is the nucleon-induced deuteron breakup. It has become obvious that to fit the $N + d$ data it is necessary to use a model derived from the Faddeev theory. Unfortunately, for systems with more than three particles we still do not have any usable model based upon rigorous theory. It is imperative to develop such a theory. However, bearing in mind the lesson learned from the $N + d$ studies we should gain understanding of the basic reactions mechanisms which will then aid in the development of such a usable model based upon rigorous theory.[1]

The prominent reaction mechanism of multiparticle reactions is the quasifree scattering (QFS). Recently, evidence has been presented that there are other quasifree (QF) processes: the quasifree reaction (QFR) mechanism in the ^{7}Li-(p, $2d$)α[2] reaction ($p + t \rightarrow d + d$ QFR), the QF process in the ^{6}Li(^{6}Li, 2α)α reaction,[3] while QF n-p capture was observed several years ago.[4]

In this paper we present a systematic study of reactions which are most favorable to establish the

role of QFR mechanisms. In our opinion these are ^{3}H + ^{3}He and ^{3}H + ^{2}H interactions which we analyze in the framework of the plane-wave impulse approximation (PWIA). We also similarly reanalyze the available data[5] on the ^{2}H(^{3}He, pt)p reaction assuming the QFR mechanism.

It is desirable to investigate the role of such QFR in a case where there are no competing strong final-state interaction (FSI) effects [e.g. α-d or α-α FSI as in the reactions ^{7}Li(p, $2d$)α and ^{6}Li-(^{6}Li, 2α)α]. If the QFR is important the data should show specific structure associated with the kinematical conditions for QFR, and if in addition the FSI effects are small and the QF pole diagram is a dominant diagram, the ratio of cross sections for several QF processes should be given by the ratio of respective free cross sections as long as the processes have the same virtual decomposition vertex [e.g. processes (a), (c), (d), and (f) in Fig. 1, ^{3}H $\rightarrow dn$]. The cross section ratio of processes with different virtual decomposition vertices might differ and the ratio might depend on detailed properties of the nuclei involved, e.g. small components of ground-state wave functions and/or short-range correlations from the hard core of the N-N interaction.

A most convenient reaction to study QFR is ^{3}H-

+ ^{3}He. Several possible QF processes with the spectator in the target (^{3}H) are shown in Fig. 1. Attractive features of these reactions are: (1) reasonably weak FSI effects, particularly in cases (b) and (c), (2) several open channels which allow one to test the relative yield of various QF processes, and (3) the QFR cross section corresponds to the enhancement in the yield where the spectator momentum $Q_s = 0$, since the ^{3}H wave function is predominantly S state.

It is also desirable to investigate the role of QFR and QFS in a case where there are strong FSI effects. In reactions such as ^{3}H(^{2}H, pt)n and ^{3}H-(^{3}He, dt)p both FSI and QF processes are important. The study of deuteron-plus-triton breakup processes[6-9] revealed the importance of nucleon-nucleon and nucleon-triton final-state interactions. Angular distributions of tritons and correlation spectra from the ^{3}He + ^{2}H → $t + p + p$ reaction have demonstrated that pickup and charge exchange are important reaction mechanisms.[5,10-12] Pronounced quasifree ^{3}He-p scattering has been observed in the ^{2}H(^{3}He, p ^{3}He)n reaction.[13] Several simple theoretical models, e.g. Watson-Migdal (WM), PWIA, plane-wave Born approximation (PWBA), and distorted-wave Born approximation (DWBA) have been used,[5,6-13] to describe the data, but it seems that neither the absolute magnitude of the cross section, nor the relative yield of various processes and often not even the shape of the spectra have been quantitatively explained. This al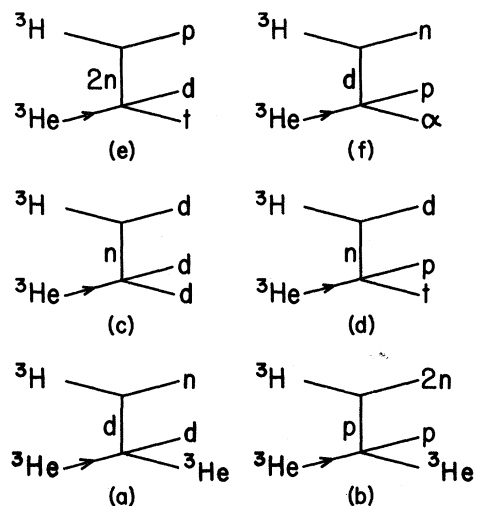l points out that the multiparticle reactions involving five nucleons are indeed very complex. There are several final-state interactions and several reaction mechanisms that are interwoven in a complex way. Nevertheless, almost paradoxically, deuteron-plus-triton breakup processes have been used to extract spectroscopic information, notably neutron-neutron scattering parameters.

The quasifree scattering of a deuteron incident on either a deuteron or a proton in a triton has not been studied. Though QFS has been observed in many reactions and at very low energies, it seemed unlikely that an important mechanism is one in
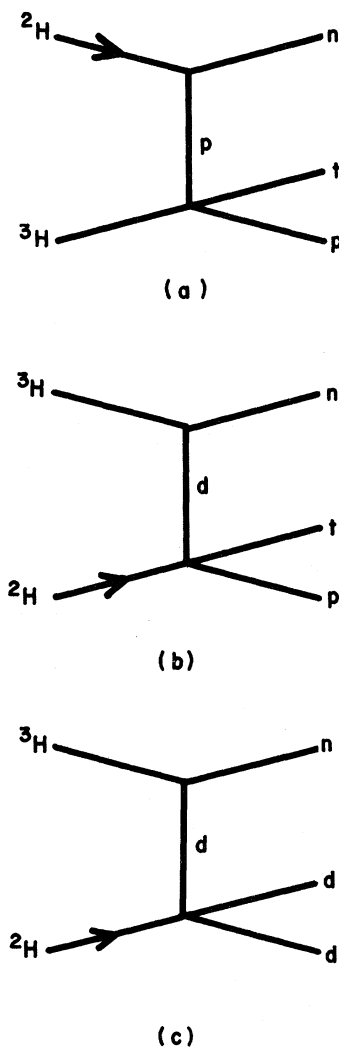

FIG. 2. Quasifree mechanisms in ^{3}H + ^{2}H interaction. (a), and (c) are QFS, while (b) is QFR. Note that in (a) the spectator is in the projectile. The spectator particle is always at the upper right of each pole diagram.

FIG. 1. QFS (a), (b) and QFR (c)—(f) in the reaction ^{3}H + ^{3}He. Note that processes (a), (f) and (c), (d) each transfer the same particle and that process (e) represents a two-neutron target. The spectator particle is always at the upper right of each pole diagram.

which a diffuse structure like a deuteron knocks
out another deuteron from a more tightly bound
triton. The QF processes involved in the ^{3}H + ^{2}H
reaction discussed in the present paper are shown
in Fig. 2.

II. THEORY

To analyze the data presented in this paper, we
use the PWIA and various forms of the tritium
wave function. The cross section in the PWIA is
expressed as

$$\frac{d^3\sigma}{dE\,d\Omega_1 d\Omega_2} = (\text{KF})|\Psi(Q_s)|^2 \sigma(\theta_{\text{c.m.}}, E)_{\text{free}}, \qquad (1)$$

where $|\Psi(Q_s)|$ is the Fourier transform of the wave
function, and KF (kinematical factor) includes the
phase-space factor. The free cross section
$\sigma(\theta_{\text{c.m.}}, E)_{\text{free}}$ for the process involved, QFS or QFR,
is determined assuming the postcollision-energy
prescription[14] and

$$\cos\theta_{\text{c.m.}} = \frac{(\vec{v}_{\text{inc}} - \vec{v}_{\text{tr}}) \cdot (\vec{v}_3 - \vec{v}_4)}{|\vec{v}_{\text{inc}} - \vec{v}_{\text{tr}}| \cdot |\vec{v}_3 - \vec{v}_4|},$$

where $\vec{v}_{\text{inc}}$, $\vec{v}_{\text{tr}}$, $\vec{v}_3$, and $\vec{v}_4$ are velocities of incident,
transferred, and two detected particles, respec-
tively [e.g. in Fig. 1(d), ^{3}He is the incident par-
ticle, the neutron is the transferred particle, and
the detected particles are p and t]. The free cross
sections were tabulated from the literature, as
will be indicated later. The forms of the wave
function we have used in the present calculation
are: (1) the overlap between the Irving-Gunn ^{3}H
wave function and the Hulthén deuteron wave func-
tion, and (2) the expression

$$u(r) \sim (e^{-gr} - e^{-br})/r \qquad (2)$$

with $b = 1.202$ fm^{-1} and $g = 0.4478$ fm^{-1} correspond-
ing to the neutron removal energy from ^{3}H or
$g = 0.5225$ fm^{-1} which corresponds to the ^{3}H bind-
ing energy. To obtain agreement between the cal-
culated and experimentally determined absolute
cross section we have used normalization factors
and/or we have introduced a radial cutoff in the
wave function given by expression (2).

III. EXPERIMENTAL

The 50-MeV ^{3}He beam and the 35-MeV ^{2}H beam
from the Naval Research Laboratory sector-fo-
cusing cyclotron are used to bombard a Ti-^{3}H
target. In one set of runs the target consists of a
layer of Ti 2.5 mg/cm^2 on a 12-mg/cm^2 gold foil
and in another set of runs the Ti layer is 4.92
mg/cm^2 on a gold foil of thickness 50 mg/cm^2.
The number of ^{3}H atoms/Ti atom is assumed to be
between 1.7 and 1.75 (information furnished by
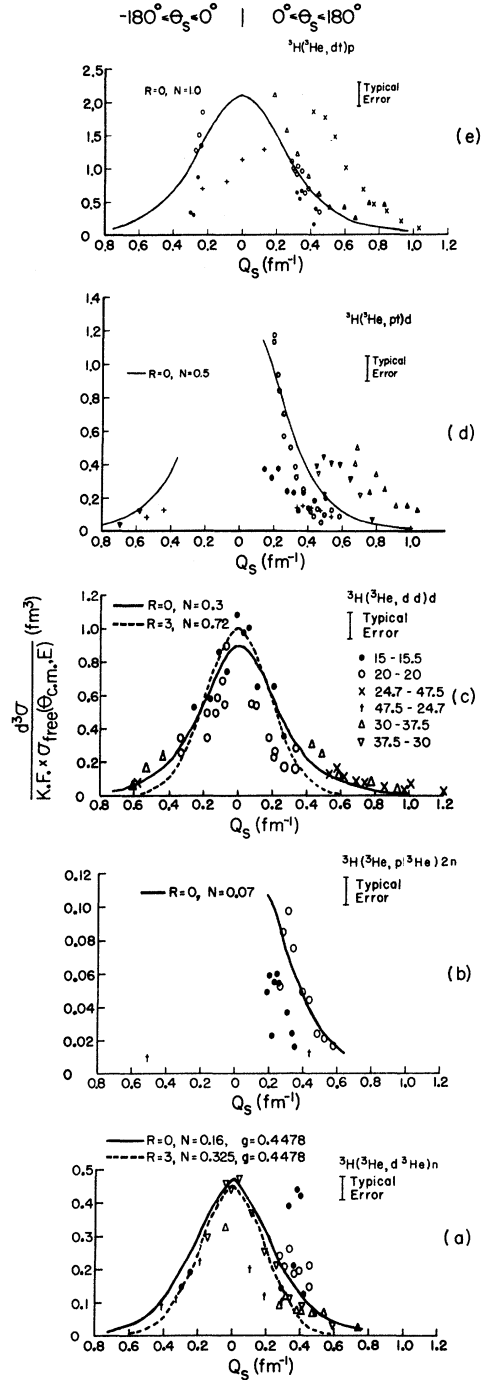supplier). Two ΔE-E counter telescopes, coplanar

FIG. 3. Data from the processes (a)−(e) of Fig. 1.
The observed cross sections are divided by the kine-
matic factor and the free cross sections for the pro-
cesses indicated. The data are then plotted as a func-
tion of the spectator momenta (Q_s) for the various angle
pairs, shown in (c). The PWIA calculations are normal-
ized (N) to fit the data. The angle of the spectator par-
ticle (θ_s) is indicated above. Note that the key for the
angle pairs is in (c) only.

and on either side of the beam are used to detect and identify charged particles. Each counter telescope has an angular resolution of 1.0° and a solid angle of 5.7×10^{-4} sr. The energy calibration, and therefore also the energy interval dE per channel, is determined from elastic ^{3}He-^{3}H scattering. Over-all, the uncertainty in the energy calibration is estimated to be ± 200 keV. Coincidence events are recorded at various pairs of angles with the ΔE and E signals stored on tape using the EMR-6050 on-line computer, thereby enabling us to measure simultaneously all processes of interest as shown in Figs. 1 or 2 for the ^{3}He and ^{2}H beam experiments, respectively.

The absolute cross section is calculated using the areal density of ^{3}H atoms as given above, the charge integrated beam, the solid angles, the energy interval, and the yield (number of counts) per channel. We estimate the absolute uncertainty in the cross section to be ±20%. Uncertainties in the relative cross sections are taken to be the statistics of the number of counts as shown in the figures.

Pairs of angles are chosen to emphasize quasi-free events (QFS and QFR), as well as NN and NT final-state interactions. Although pairs of angles are selected to emphasize certain interactions, it is possible on repetitive tape playback to obtain information on ^{3}He or ^{2}H induced reactions for all angle pairs via the software particle identification. During a run the coincidence events between a selected pair of particles are displayed via hardware particle identification.

The ΔE counter thicknesses are chosen to optimize the detection limits for all reactions observed, although in specific cases other thicknesses would improve the experimental situation.

The background is determined from the recorded

events near the kinematic locus. There are cases where the cross sections for the breakup of the projectile in the field of a heavy nucleus (in this case titanium and gold) is large and, therefore, this background could be important. However, for all correlated pairs presented in this work, background is negligible.

IV. RESULTS AND DISCUSSION

In all the reactions studied in this work we find pronounced enhancements corresponding to QF processes. To correlate data obtained at different angles we present them in a form of the square of the nucleon-deuteron or nucleon-dinucleon pair cluster momentum wave function $|\Psi(Q_s)|^2$ of ^{3}H using the PWIA. From Eq. (1) it can be seen that by dividing the observed cross section by the kinematic factor and the free cross section, the momentum form of the wave function is obtained. If the quasifree process is important, the data from various angle pairs should be consistent for the same spectator momentum Q_s and should show a pronounced enhancement at $Q_s = 0$. The results are plotted in Fig. 3. Figure 3(a)–3(e) corresponds to Fig. 1(a)–1(e). Similarly, the neutron-deuteron cluster momentum wave function of ^{3}H is extracted from the ^{3}H(^{2}H, dd)n data as shown in Fig. 4.

The various reactions we have studied are discussed separately below. Table I lists these reactions, the mechanism involved (which can be seen in Figs. 1 and 2) and the references for the data sets used in the PWIA calculation. Detailed balance is used when the available data set is for the inverse reaction.

A. ^{3}H(^{3}He,d^3He)n Reaction

This is a case of QFS. An example of cross-section data is shown in Fig. 5 for the angle pair θ_d

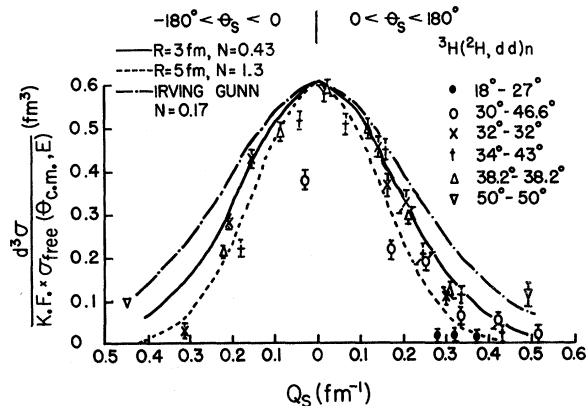FIG. 4. The square of the neutron-deuteron cluster momentum wave function of ^{3}H from the ^{3}H(^{2}H,dd)n data. The angle of the spectator particle is indicated above.
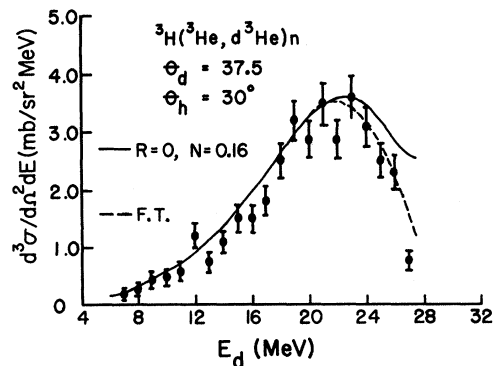

FIG. 5. A comparison of observed cross section and various calculations for the ^{3}H(^{3}He,d^3He)n reaction. Here F.T. is the Fourier transform.

TABLE I. Summary of elastic scattering and reaction cross-section data used in PWIA calculations.

Reaction mechanism	Energy, lab	c.m. angle	Source	Reaction mechanism	Energy, lab	c.m. angle	Source
$^3H(^3He, d\,^3He)n$	E_{3He} =4.0	70°–115°	Extrapolated	$^3H(^3He, dd)d$	E_d =0.156	60°–120°	Bennet *et al.*[k]
$^3He + d \to\,^3He + d$	8.4	16.7°–160°	Brolley *et al.*[a]	$^3He + n \to d + d$			
	12.42	16.7°–160°		$^3H(^2H, pt)n$ as			
	18.08	35°–150°	King and	$p + t \to d + d$			
	19.4	35°–150°	Smythe[b]		0.96	47°–133°	Blair *et al.*[m]
	20.68	35°–150°			3.02	51°–129°	
	25.0	35°–150°			5.8	22°–158°	Brolley and Fowler[n]
	30.55	35°–150°					
	34.60	35°–150°			8.15	22.9°–157°	Brolley *et al.*[o]
	39.63	35°–150°			10.4	23.6°–156.4°	
	41.63	35°–150°			12.2	24°–156°	
	43.73	35°–150°			13.8	24.3°–155.7°	
	52.5	35°–170°	Extrapolated		16.6	25°–155°	Fegley and Cahill[j]
$^3H(^3He, p\,^3He)2n$ and	E_{3He} =7.14	67°–135°	Drigo *et al.*[c]		19.4	31.7°–148.3°	
$^2H(^3He, p\,^3He)n$	10.62	67°–135°			24.5	18.9°–161.1°	
$^3He + p \to\,^3He + p$	16.53	27.6°–166.6°	Clegg *et al.*[d]		26.6	11.4°–162°	
	25.53	27.6°–166.6°			32.5	15.3°–162.4°	
	34.4	27.6°–166.6°		$^3H(^3He, pt)d$ and	E_p =2.45	30°–160°	Willard *et al.*[p]
	40.8	16°–172°	Hutson *et al.*[e]	$^2H(^3He, pt)p$			
	49.8	16°–173.3°		$^3He + n \to p + t$	4.9	30°–160°	Wilson *et al.*[q]
	58.4	20°–166.6°			7.43	30°–160°	
	93.0	16.1°–166.6°	Kim *et al.*[f]		10.42	30°–160°	
$^3H(^2H, pt)n$	E_p =2.12	58.6°–168°	Classen *et al.*[g]		12.9	30°–160°	
$p + t \to p + t$	3.5	55°–169°			26.7	30°–160°	Extrapolated
	6.5	20°–160°	Brolley *et al.*[a]	$^3H(^3He, p\alpha)n$	E_d =5.9	11.7°–146.2°	Stewart *et al.*[r]
	8.3	20°–160°		$^3He + d \to p + \alpha$	7.5	23.72°–169.8°	
	13.6	20°–170°	Detch *et al.*[h]		10.4	18.1°–174°	
	16.23	20°–170°			12.3	18.3°–170.2°	
	19.48	20°–170°			13.7	18.4°–170.4°	
	26	26.7°–166°	Extrapolated		24.7	30°–120°	Bilaniuk and Slobodrian[s]
$^3H(^2H, dd)n$	E_d =6.0	30°–150°	Wilson *et al.*[i]		27	30°–180°	
$d + d \to d + d$	8.2	20°–160°			40	30°–150°	Extrapolated
	9.53	40°–140°			65	30°–150°	
	10.55	40°–140°		$^3H(^3He, dt)p$	E_{3He} =5	30°–145°	There is no available data. Angular distribution data are available for the reaction $^2H(^3He,t)$-$2p$, E_{3He}=17.5 and 21 MeV (Ref. 16) and E_{3He}=60 MeV (Ref. 17). See text.
	12.1	20°–160°		$^3He + 2n \to d + t$	10	30°–145°	
	14.7	30°–149.9°	Fegley and Cahill[j]		20	30°–145°	
	16.6	30.1°–149.9°			30	30°–145°	
	20.9	30.1°–149.9°			40	30°–145°	
	24.5	30.1°–149.9°			50	30°–145°	
	26.6	30.1°–149.8°			60	30°–145°	
	31.6	30.1°–149.8°					
	34.9	30.1°–149.9°					

[a] J. E. Brolley *et al.*, Phys. Rev. 117, 1307 (1960).
[b] T. R. King and R. Smythe, Nucl. Phys. A183, 657
[c] L. Drigo *et al.*, Nucl. Phys. 89, 632 (1966).
[d] T. B. Clegg *et al.*, Nucl. Phys. 50, 621 (1964).
[e] R. L. Hutson *et al.*, Phys. Rev. C 4, 17 (1971).
[f] C. C. Kim *et al.*, Nucl. Phys. 58, 32 (1964).
[g] R. S. Classen *et al.*, Phys. Rev. 82, 589 (1957).
[h] J. L. Detch *et al.*, Phys. Rev. C 4, 52 (1971).
[i] A. S. Wilson *et al.*, Nucl. Phys. A126, 193 (1969).
[j] R. W. Fegley and T. A. Cahill, to be published; private communication.

[k] W. E. Bennet *et al.*, Phys. Rev. 69, 418 (1946).
[m] J. M. Blair *et al.*, Phys. Rev. 74, 1594 (1948).
[n] J. E. Brolley and J. L. Fowler, in *Fast Neutron Physics*, edited by J. B. Marion and J. L. Fowler (Interscience, New York, 1960), Vol. I.
[o] J. E. Brolley *et al.*, Phys. Rev. 107, 820 (1957).
[p] H. B. Willard *et al.*, Phys. Rev. 90, 865 (1953).
[q] W. E. Wilson *et al.*, Nucl. Phys. 27, 421 (1961).
[r] L. Stewart *et al.*, Phys. Rev. 119, 1649 (1960).
[s] O. M. Bilaniuk and R. J. Slobodrian, Nucl. Phys. 50, 585 (1964).

$=37.5°$ and $\theta_{3_{He}} = 30°$. This angle pair enhances the QF condition for this reaction. The solid curve is the PWIA prediction using for the nucleon-deuteron wave function expression (2) with $g = 0.4478$ fm^{-1} and a normalization factor $N = 0.16$. An identical curve is obtained using the overlap between the ^{3}H Irving-Gunn wave function and the Hulthén deuteron wave function with a normalization factor $N = 0.13$.

At this point it is worthwhile mentioning that the position of the maximum in calculated spectra is determined by both the Fourier transform and the free cross section, and indeed at some angle pairs (20°-20°, 15°-15°) for the ^{3}H(^{3}He, $d\,^3$He)n reaction the positions of the PWIA and Fourier transform maxima are as much as 6 to 8 MeV apart. The data always follow the PWIA prediction, thereby providing some support for the assumption of the postcollision-energy prescription which has been used in the present calculations.

A reasonable fit to the composite data [see Fig. 3(a)] is obtained if one describes the nucleon-deuteron wave function with expression (2) where g $= 0.4478$ fm^{-1}, and a normalization factor $N = 0.16$ is used. A cutoff radius with $R = 3$ to 4 fm seems to give a better fit to the shape. These values for N and R are in good agreement with data on QFS.[15]

The enhancement at $Q_s = 0.4$ fm^{-1} (for 15°-15°) indicates that another process may contribute to the cross section. However, this evidence is uncertain since for $\theta_d = \theta_{3_{He}} = 15°$, we had to extrapolate existing data to obtain cross sections necessary to make the calculation (see Table I).

B. ^{3}H(^{3}He,$p\,^3$He)$2n$ Reaction

This is also a QFS. In Fig. 6 we show the data projected on the E_p axis for $\theta_p = \theta_{3_{He}} = 20°$, together with the PWIA prediction using Eq. (2) for the ^{3}H wave function with $g = 0.5225$ fm^{-1} and a normal-
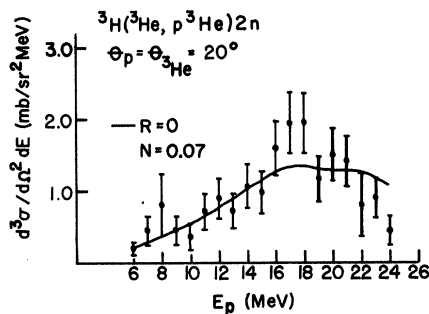

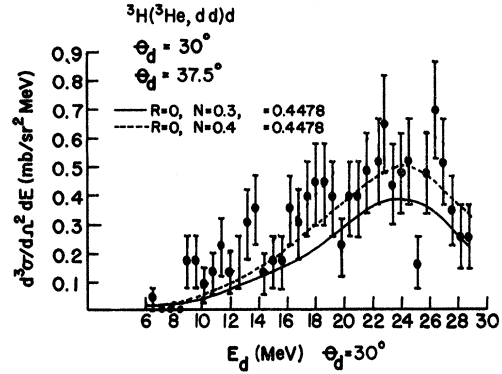
FIG. 7. A comparison of the observed cross section and PWIA calculation for the reaction ^{3}H(^{3}He,dd)d. Two different normalization factors $N = 0.3$ and $N = 0.4$ are shown.

ization of 0.07. Note that the peak in the PWIA coincides closely with the peak in the data. The peak in the Fourier transform comes at about 23 MeV, but the free cross section is dropping about a factor of $2\frac{1}{2}$ from 16 to 26 MeV, which is sufficient to bring the experimentally observed peak to its observed value, thus again giving credence to the PWIA and the use of the postcollision-energy prescription to determine the correct free cross section.

Kinematical conditions for p-^{3}He QFS [Fig. 3(b)] correspond to very forward angles, and thus we studied this process only for $Q_s \geq 0.2$ fm^{-1}. We were able to use the data from the angle pairs 15°-15°, 20°-20°, and 47.5°-24.7°. At other angle pairs the cross section for the ^{3}H(^{3}He,$p\,^3$He)$2n$ reaction is very low. In this Q_s domain, it appears that the data agree with the assumption of the QFS. Both 15°-15° and 20°-20° show the proper QFS enhancement, though there is a difference in the absolute magnitude, which is somewhat outside our

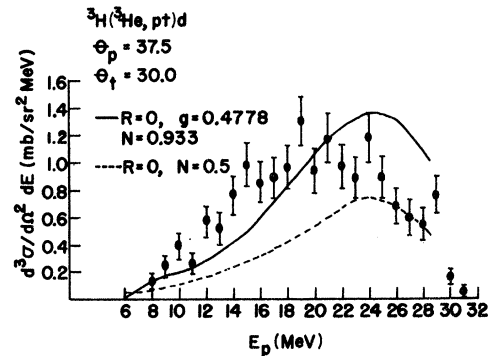FIG. 6. A comparison of observed cross section and PWIA calculation for the reaction ^{3}H(^{3}He,$p\,^3$He)$2n$.

FIG. 8. A comparison of the observed cross section and PWIA calculations for the reaction ^{3}H(^{3}He,pt)d. Two different normalization factors $N = 0.933$ and $N = 0.5$ are shown.

absolute cross section measurements. To obtain the fit we used a normalization factor of 0.07 and we assumed that the p-$2n$ relative motion is represented by Eq. (2) using $g=0.5225$ fm^{-1} (which corresponds to the ^{3}H binding energy).

C. ^{3}H(^{3}He,dd)d Reaction

This is the first of the QFR we have studied in the ^{3}H-^{3}He interaction. An interesting feature of this reaction is that it was easily seen experimentally in all angle pairs, even those far away from the QF region. The ^{3}H momentum wave function extracted from the data is shown in Fig. 3(c). A typical spectrum is shown in Fig. 7. A reasonable fit is obtained if one describes the nucleon-deuteron wave function with expression (2) and uses a normalization factor $N=0.3$, with $g=0.4778$ fm^{-1}.

The effect of d-d FSI is very weak, and we found no evidence of it in any of the spectra.

Another interesting feature of this $n+{}^3$He $\rightarrow$ $d+d$ QFR is that it leads also to the unbound n-p system. In particular, we see evidence for the reaction ^{3}H(^{3}He, dd)d^*, which is separated kinematically from the ^{3}H(^{3}He, dd)d reaction by ~2 MeV. The cross section for d^* is low and comparable to similar four-body breakup cross sections.

D. ^{3}H(^{3}He,pt)d Reaction

This is another QFR. Figure 8 shows the observed cross section plotted as a projection on the proton axis for the angle pair $\theta_p=37.5°$, and $\theta_t=30°$. Also shown are the PWIA predictions assuming for the ^{3}H wave function expression (2), with $g=0.4778$ fm^{-1}, and normalization factors of 0.93 and 0.5.

As in the ^{3}H(^{3}He,p ^{3}He)$2n$ QFS process kinematical conditions for QFR in the ^{3}H(^{3}He,pt)d reaction correspond to forward angles so we studied this reaction only for angle pairs giving $Q_s > 0.2$ fm^{-1}. The ^{3}H momentum wave function extracted from the data is shown in Fig. 3(d). A reasonable fit

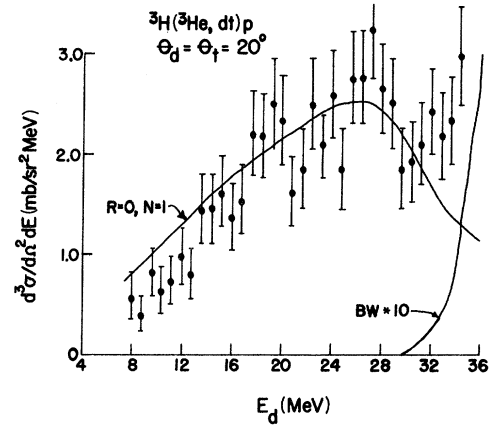FIG. 9. Data from the ^{3}H(^{3}He,dt)p reaction and PWIA calculations. The rise in the data near 35 MeV can be explained by the 22-MeV state in ^{4}He shown by the calculated curve BW (Breit-Wigner expression to describe the pt FSI).

to the data from all angle pairs is given using $N=0.5$ and $g=0.4778$ fm^{-1}. We saw no evidence for FSI effects in any of the spectra.

E. ^{3}H(^{3}He,dt)p Reaction

This process can proceed through the QFR mechanism when there is effectively a two-neutron "target" [see Fig. 1(e)].

In Fig. 9 we show the observed cross section for the ^{3}H(^{3}He, dt)p reaction at the angle pair $\theta_d=\theta_t =20°$. The peak in the Fourier transform for this reaction occurs at about 32 MeV, but the data appear to peak at about 26 MeV, essentially as predicted by the PWIA. The rise in the data near 34 MeV can be explained by the t-p FSI due to the 22-MeV state in ^{4}He*. This rise is shown by the curve BW which is calculated from the Breit-Wigner expression with the parameters of the 22-MeV state: $E_R^{pt} =2.14$ MeV, $\Gamma =2$ MeV.

In contrast to the reactions previously discussed, the ^{3}H(^{3}He, dt)p reaction shows dominant t-p FSI.

TABLE II. ^{3}H(^{2}H, ^{3}He)$2n$ data generated from ^{3}He(^{2}H, t)$2p$ data at $E_t =17.5$, 21, and 60 MeV, assuming the energy dependence of ^{2}H-^{3}He elastic scattering data.

c.m. angle (deg) \ Energy E_{3He} (MeV)	5	10	20	30	40	50	60
			Differential cross section (mb/sr)				
30	78	27	3.9	1.1	0.77	0.52	0.27
45	20	6.2	1.08	0.8	0.72	0.45	0.23
60	2.4	2.4	1.95	1.3	0.74	0.37	0.10
75	0.7	1.7	1.7	0.84	0.44	0.21	0.08
90	0.62	1.5	1.5	0.7	0.33	0.13	0.04
105	1.5	1.8	1.22	0.84	0.66	0.40	0.19
120	4.4	2.5	1.58	1.16	0.98	0.69	0.37
135	0.98	2.2	2.35	1.7	1.2	0.80	0.58
145	1.10	2.4	3.0	2.35	1.75	1.35	0.89

TABLE III. Summary of the data and reaction mechanisms. The transferred particle is the second particle listed in column mechanism.

Experiment/Theory	Cross section		Mechanism	Figure
Quasifree scattering				
^{3}H(^{3}He, d ^{3}He)n	0.14	±0.03	^{3}He + d → ^{3}He + d	1(a)
^{3}H(^{3}He, p ^{3}He) 2n	0.07	±0.03	^{3}He + p → ^{3}He + p	1(b)
^{3}H(^{2}H, pt)n	0.06	±0.03	$t + p$ → $t + p$	2(a)
^{3}H(^{2}H, dd)n	0.17	±0.01	$d + d$ → $d + d$	2(c)
^{2}H(^{3}He, ^{3}Hep)n	0.21	±0.08	^{3}He + p → ^{3}He + p	14(a)
Quasifree reactions				
^{3}H(^{3}He, dd)d	0.3	±0.03	^{3}He + n → $d + d$	1(c)
^{3}H(^{3}He, dd)$d*$	0.045	±0.030	^{3}He + n → $d + d$	1(c)
^{3}H(^{3}He, pt)d	0.5	±0.2	^{3}He + n → $p + t$	1(d)
^{3}H(^{3}He, dt)p	1.0	±0.6	^{3}He + 2n → $d + t$	1(e)
^{3}H(^{3}He, $p\alpha$)n	0.10	±0.07	^{3}He + d → $p + \alpha$	1(f)
^{3}H(^{2}H, pt)n	1.3	±0.6	$d + d$ → $p + t$	2(b)
^{2}H(^{3}He, tp)p	0.53	±0.15	^{3}He + n → $p + t$	14(b)

The data presented in Fig. 3(e) for the ^{3}H(^{3}He, dt)p are those for which $|E_{p-t}^{rel} - E_{res}| \geq 3$ MeV, thereby excluding the effect of the p-t FSI due to states in ^{4}He just above the p-t threshold. The quantity E_{res} is the p-t relative energy corresponding to the 22-MeV ^{4}He* state. One should stress that the data as presented in Fig. 3(e) are subject to a large uncertainty due to the complete absence of the ^{3}H(^{2}H, ^{3}He)2n cross-section data needed as an input in the PWIA calculation. Only two measurements of angular distributions of the charge symmetric reaction ^{3}He(^{2}H, t)2p exist.[16, 17] We generated[18] the data set for ^{3}H(^{2}H, ^{3}He)2n reaction (see Table II), assuming that the energy variation of ^{3}H(^{2}H, ^{3}He)2n data would be similar to existing d-^{3}He elastic scattering data, and that the absolute cross sections for ^{3}H(^{2}H, ^{3}He)2n data at $E_{3_{He}}$=17.5, 21, and 60 MeV are equal to those in Refs. 16 and 17.

F. ^{3}H(^{3}He,$p\alpha$)n Reaction

This process is dominated by the nucleon-α FSI. We do, however, see evidence for the QFR mechanism illustrated in Fig. 1(f). The cross section is very low and we summarize these results in Table III only.

G. ^{3}H(^{2}H,dd)n Reaction

The d-d QFS process dominates this reaction and there are no FSI effects. Indeed, the data show QFS behavior even for Q_s as large as 0.5 fm^{-1}.

Cross-section data for the ^{3}H(^{2}H, dd)n reaction are shown in Fig. 10 for the angle pair θ_d = 34°,

θ_d = 43.3°. Note that the use of a radial cutoff in expression (2) more nearly explains the shape and magnitude of the data than does the use of the overlap of the Irving-Gunn and Hulthén functions.

The composite data are compared in Fig. 4 with the calculation using the Irving-Gunn ^{3}H wave function with the Hulthén deuteron wave function in the PWIA. Again, this combination does not do as well in both shape and magnitude as does the use of expression (2) for the ^{3}H wave function (where g=0.4478 fm^{-1}) with a cutoff radius of 4 fm.

The value of the normalization factor for the Irving-Gunn wave function, or equivalently the cutoff radius, are in agreement with those found in ^{2}H(^{1}H, 2p)n and ^{3}He(^{1}H, pd)p reactions.[15]
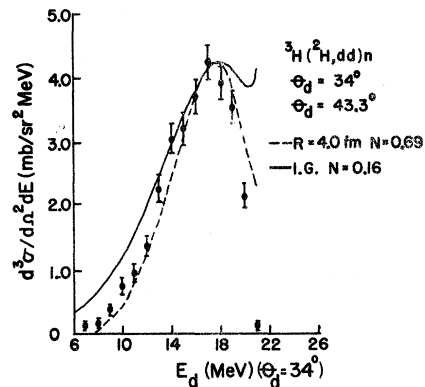

FIG. 10. Experimental cross sections and PWIA calculations for the reaction ^{3}H(^{2}H,dd)n.
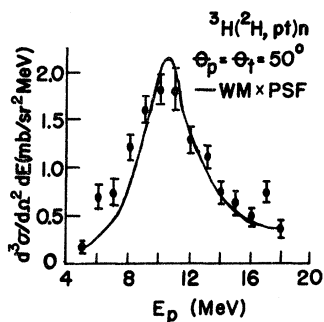
FIG. 11. Spectra at $\theta_p = \theta_t = 50°$. Solid curves are WM predictions using only $^1S_0$ FSI.

H. $^3H(^2H,pt)n$ Reaction

This is the case where many reaction mechanisms are important and are interwoven with various FSI.

An example of the $n-p$ FSI enhancement in this reaction is shown in Fig. 11. The kinematical conditions $(\theta_p = \theta_t = 50°)$ were chosen so that one is far from $n-t$ QFS, and a good agreement is obtained between the data and the WM model using only $^1S_0$ FSI and known singlet effective range parameters. A summary of all $^3H(^2H,pt)n$ data is shown in Fig. 12 as a ratio of the cross section and the phase-space factor (PSF) as a function of the $n-p$ relative energy (see Fig. 4 for a list of angle pairs studied). One concludes that only data with $E_{np} \leqslant 1$ MeV are in agreement with the WM model, even if one chooses data far from dominant $n-t$ FSI and $p-t$ QFS (see Fig. 12).

A similar plot of $d^3\sigma/PSF$ as a function of $n-t$ relative energy does not show any pronounced peaks, even if $p-t$ QFS and $n-p$ FSI kinematical regions are removed. Individual spectra sometimes show enchancements that could be due to the
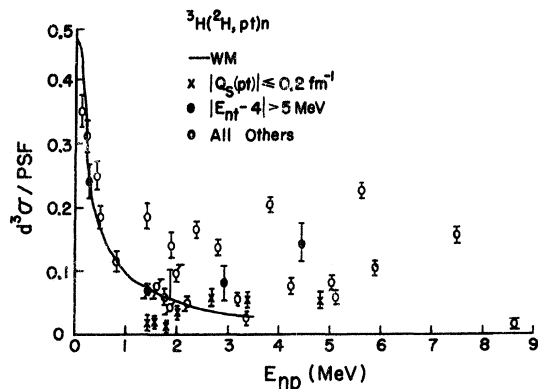
^4H level about 3.4 MeV above the $n-t$ mass with $\Gamma \approx 5$ MeV. However, the poor fit of these spectra suggests that the enhancement represents a complex interplay of $n-t$ FSI and various reaction mechanisms.

To investigate the contribution of $p-t$ QFS, the neutron in the projectile being the spectator [see Fig. 2(a)] the data are presented in Fig. 13(a) as experimental differential cross section divided by kinematical factors and free $p-t$ cross section as a function of momentum transfer. The solid curve is the square of the Fourier transform of the deuteron Hulthén wave function. It is obvious that though in some cases $p-t$ QFS is important, as the peak at $Q_s = 0$ shows, there are other reaction mechanisms (peak at $Q_s = 1$ fm^{-1}) which also play important roles. The peak at $Q_s = 1$ fm^{-1} is not due either to $n-p$ or to $n-t$ FSI. A possible reaction mechanism could be the quasifree $dd \rightarrow pt$ reaction with a neutron in the target being the spectator [see Fig. 2(b)]. Figure 13(b) shows the data
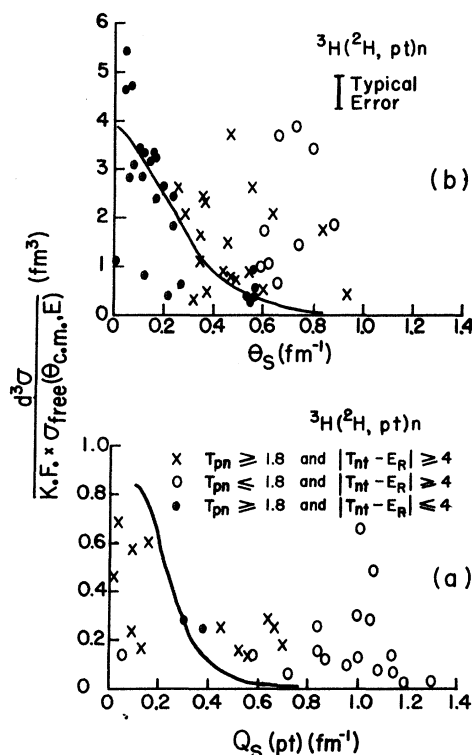

FIG. 12. The $^3H(^2H,pt)n$ cross section divided by the phase-space factor as a function of $n-p$ relative energy for all angles studied.

FIG. 13. (a) Square of the deuteron momentum wave function extracted from the $^3H(^2H,pt)n$ data, assuming $p-t$ QFS. (b) The square of the neutron-deuteron momentum wave function of ^3H extracted from the $^3H-(^2H,pt)n$ data, assuming the $dd \rightarrow pt$ quasifree reaction. Solid curves are predictions using the Hulthén wave function $R = 0$, and normalization factors $N = 0.06$ (a), $N = 1.3$ (b), respectively.
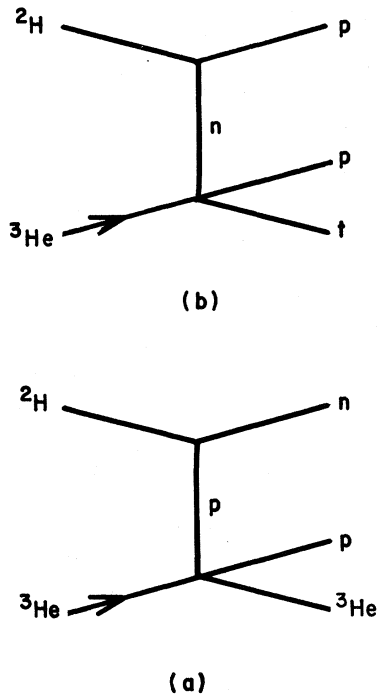
(b)

(a)

FIG. 14. QFS (a) and QFR (b) in the reaction ^{2}H + ^{3}He. The spectator particle is always at the upper right of each pole diagram.

presented as the square of the n-d cluster momentum wave function of ^{3}H. If one excludes the contribution of the n-p FSI kinematical domain ($T_{pn} \leqslant 1.8$ MeV), one can conclude that the quasifree $dd \rightarrow pt$ reaction mechanism may be an important contribution. It should be mentioned that the ratio of the experimentally observed yield and the theoretically predicted p-t QFS is 0.06, while the analogous ratio for the $dd \rightarrow pt$ QFR is 1.9.

I. Other Evidence for QFR

Warner et al.[5] showed evidence for intense spectator proton peaks in the reaction ^{2}H(^{3}He, tp)p. Assuming that the process proceeds as a ^{3}He(n, p)t QFR [see Fig. 14(b)] and using ^{3}He(n, p)t free cross sections in the PWIA, we were able to predict correctly the shape of the spectra using the same normalization factor of 0.53 for both $\theta_t = 15°$, $\theta_p = 25°$ and $\theta_t = 15°$, $\theta_p = 44°$, which the model used in Ref. 5 could not explain.

V. SUMMARY AND CONCLUSION

The fact that the data in Sec. IV. A–I, analyzed assuming the dominance of pole graphs (see Figs. 1, 2, and 14) reveal pronounced enhancements at momentum transfer $Q_s = 0$, provides clear evidence for the importance of QFS and QFR mechanisms.

We conclude, therefore, that a successful model of these multiparticle reactions should include such processes as QFR and d-d QFS, which none of the phenomenological models have done to date so far. This does not imply that other diagrams are not important even for these specific kinematic conditions chosen so as to emphasize QF processes. Many tests have been performed[1,15,19] to determine the relative importance of pole graphs. In the study of nucleon induced deuteron breakup clear evidence that the pole diagram is not the dominant term has come from the comparison of absolute ^{2}H(^{1}H, $2p$)n and ^{2}H(^{1}H, pn)p cross sections. Therefore, we believe that the importance of the pole diagrams studied in the present work should be similarly tested.

In Table III we summarize the work reported in this paper and our analysis of the work reported in Ref. 5. The errors assigned to the ratios of experimental to theoretical cross sections represent our estimate of the over-all uncertainty.

It is obvious that the ratios of experimental to theoretical cross sections given in Table III are quite different, varying from about 0.05 ± 0.03 to 1.3 ± 0.6. However, three different incident channels (^{3}H + ^{3}He, ^{2}H + ^{3}H, and ^{2}H + ^{3}He) and three different virtual decomposition vertices are presented in Table III, and one would not expect all of them to yield the same ratio.

If we group the reactions according to the virtual decomposition vertex, we see that within each group the ratios are inconsistent:

reactions 1, 4, 6, 8, 10, 11: ^{3}H → nd vertex;

reactions 2, 7, 9: ^{3}H → nnp vertex;

reactions 3, 5, 12; ^{2}H → np vertex.

However, if we subgroup according to transferred particle we find that the ratios are significantly smaller if the transferred particle is charged. Moreover, there is a tendency for the ratios to be in agreement if the reactions are grouped according to whether the transferred particle is charged or uncharged. For example, ratios for the reactions 1, 2, 3, 4, 5, and 10 are similar and all smaller than the ratios for reactions 6, 8, and 12, which are similar to each other. For two reactions, 9 and 11, the ratios are very large. The large uncertainty quoted for the ratio of reaction 9 stems from the absence of ^{3}H(^{2}H, ^{3}He)$2n$ cross-section data and it is quite possible for this ratio to be very different from the value listed. For the reaction ^{3}H(^{2}H, pt)n the ratio may have no significance as an examination of Fig. 13 suggests no clear evidence for appreciable QFR contribution.

It should be pointed out that in general the ratio is larger for QFR than for QFS processes. Even

if the ratios for processes 9 and 11 are discarded because of large uncertainties, the ratios of experimental to theoretical cross sections for QFR are more than twice that for QFS.

The discrepancies and regularities discussed above could not be correlated with the influence of the various FSI.

Table III demonstrates that the PWIA does not correctly predict the absolute magnitude of the cross section [except for the ^{3}H(^{3}He, dt)p reaction which could be fortuitous].

It is possible that some processes reported in this work are constrained to be peripheral and thus the number of two-body collisions is limited and the multiscattering series is less divergent. This could account for a reasonably good Fourier transform extracted from the data and for normalization factors close to 1. The reason for the peripheral nature of these processes could be related to the fact that very large structures, e.g. $2n$ or d, have to be transferred and it is most likely to find them in the tail of the ^{3}H wave function.

Though the enhancements at $Q_s = 0$ indicate the significance of QFR mechanisms, since there are serious discrepancies in the absolute magnitudes, and since the Treiman-Yang criterion[20] is probably not fulfilled,[21] we conclude that, in much the same way as for the $N + d$ system, the multiple scattering series presumably does not converge and a rigorous theoretical treatment is needed.

The appreciable cross sections observed for processes where in the pole diagram a transferred particle is a two-nucleon system (deuteron or n-n pair) indicates the importance of nucleon-nucleon correlations in the ^{3}H ground-state wave function.

In our analysis we did not include all pole diagrams. For example, the reaction ^{3}H(^{3}He, $d\,^3$He)n can proceed as a ^{3}He-^{2}H QFS [Fig. 1(a)] but also as ^{3}He-n QFS (d in the target acts as a spectator, $E_d \approx 0$) as ^{3}H + $2p \rightarrow d + ^3$He QFR (n in the projectile acts as a spectator, $E_{^3\mathrm{He}} \approx \frac{1}{3} E_{\mathrm{inc}}$ and $\theta_n \approx 0$), and as ^{1}H + ^{3}H $\rightarrow n + ^3$He QFR (d in the projectile acts as spectator, $E_d \approx \frac{2}{3} E_{\mathrm{inc}}$ and $\theta_d \approx 0$) and though we have selected kinematic conditions to enhance the ^{3}He-^{2}H QFS in this particular case, the interference curves between various pole graphs might be quite important.[22] One is led to the conclusion that if the QFR mechanism is important as our results seem to indicate, then what we assumed so far to be only a QFS (involving complex particles) is even in the picture of pole graphs a complex interplay of QFS and QFR.

ACKNOWLEDGMENTS

[1]*Proceedings of the International Conference on Few Particle Problems in the Nuclear Interaction,* edited by I. Slaus *et al.* (North-Holland, Amsterdam, 1973).

[2]M. Furić, R. K. Cole, H. H. Forster, C. C. Kim, D. Y. Park, J. Rucker, H. Spitzer, and C. N. Waddell, Phys. Lett. **39B**, 629 (1972).

[3]L. L. Gadeken and E. Norbeck, Phys. Rev. Lett. **27**, 952 (1971); to be published.

[4]P. M. Koehler, K. W. Rothe, and E. H. Thorndike, Phys. Rev. Lett. **18**, 933 (1967).

[5]R. E. Warner, G. C. Ball, W. G. Davies, A. J. Ferguson, and J. S. Forster, Phys. Rev. Lett. **27**, 961 (1971).

[6]P. D. Parker, P. F. Donovan, J. V. Kane, and J. F. Mollenauer, Phys. Rev. Lett. **14**, 15 (1965).

[7]R. W. Zurmühle, Nucl. Phys. **72**, 225 (1965).

[8]R. E. Warner, B. E. Corey, E. L. Petersen, R. W. Bercaw, and J. E. Poth, Nucl. Phys. **A148**, 503 (1970).

[9]A. Niiler, R. J. Spiger, W. Von Witsch and G. C. Philips, Nucl. Phys. **A179**, 263 (1972).

[10]H. E. Conzett, E. Shield, R. J. Slobodrian, and S. Yamabe, Phys. Rev. Lett. **13**, 625 (1964).

[11]M. Jakobson, J. H. Manley, and R. H. Stokes, Nucl. Phys. **70**, 97 (1965).

[12]E. M. Henley, F. C. Richards, and D. U. L. Yu, Nucl. Phys. **A103**, 361 (1967).

[13]P. A. Assimakopoulos, E. Beardsworth, D. P. Boyd, and P. F. Donovan, Nucl. Phys. **A144**, 272 (1970).

[14]P. Gaillard, M. Chevallier, J. Y. Grossiord, A. Guichard, M. Gusakow, J. R. Pizzi, and J. P. Maillard, Phys. Rev. Lett. **25**, 593 (1970).

[15]I. Slaus, Invited Paper, International Symposium on Three-Body Problems and Related Topics, Budapest, 1971 (unpublished).

[16]M. Jakobson, J. H. Manley, and R. H. Stokes, Nucl. Phys. **70**, 97 (1965).

[17]R. W. Rutkowski, ORNL Report No. ORNL-TM-3484 (unpublished).

[18]The present data set for the reaction ^{3}H(^{2}H, ^{3}He)$2n$ differs from the one used in the preliminary report of this work at the International Conference on Few Particle Problems in the Nuclear Interaction, Los Angeles, 28 August–1 September, 1972 (unpublished). We believe that the present data set is superior since additional ^{3}He(^{2}H, t)$2p$ data (i.e., 17.5-MeV data) and ^{2}H-^{3}He data from $E_{^3\mathrm{He}} = 35$–44 MeV are included and connected with the $E_{^3\mathrm{He}} = 60$ MeV ^{3}He(^{2}H,t)$2p$ data.

[19]G. V. Avakov, E. F. Kolinsky, and V. V. Turovtsev, Nucl. Phys. **A196**, 529 (1972).

[20]S. B. Treiman and C. N. Yang, Phys. Rev. Lett. **8**, 140 (1962).

[21]R. E. Warner and J. S. C. McKee, private communication on the basis of data in Ref. 5.

[22]The interference between the ^{3}He + 2$n \rightarrow d + t$ QFR in the reaction ^{3}H(^{3}He, dt)p and the p-t QFS with the deuteron in the projectile acting as a spectator could be one of the reasons for a large cross section observed experimentally for this reaction.